ECCOMAS Congress 2016
VII European Congress on Computational Methods in Applied Sciences and Engineering
M. Papadrakakis, V. Papadopoulos, G. Stefanou, V. Plevris (eds.)
Crete Island, Greece, 5–10 June 2016

EFFECTIVE MESO AND MACRO PROPERTIES FOR FIBRE-REINFORCED-POLYMER CURING COUPLED TO VISCO-ELASTICITY

R. Mahnken[1] **and C. Dammann**[2]

[1],[2]Chair of Engineering Mechanics (LTM)
University of Paderborn
Warburger Str. 100, 33098 Paderborn, Germany
[1]e-mail: mahnken@ltm.upb.de
[2]e-mail: dammann@ltm.upb.de

Keywords: Curing, shrinkage, thermal-mechanical-chemical-coupling, homogenization, RVE.

Abstract. *Our work presents a three-scale model for temperature-dependent visco-elastic effects accompanied by curing, which are important phenomena in a resin transfer molding (RTM) process. The effective bulk quantities in dependence on the degree of cure are obtained by homogenization for a representative unit cell (micro-RVE) on the heterogeneous microscale. To this end, an analytic solution is derived by extension of the well known composite spheres model. Voigt and Reuss bounds resulting from the assumption of a homogeneous matrix are compared to the effective quantities. During curing and subsequent mechanical loading, the periodic mesostructure defined by a visco-elastic polymeric matrix and linear-thermo-elastic carbon fibres is taken into account as a representative unit cell (meso-RVE) subjected to thermo-mechanical loading on the mesoscale. Homogenization of the mesoscale by volume averaging is applied to obtain the effective properties for the fully cured composite on the macroscale, e.g. the macroscopic anisotropic thermal expansion coefficient. In the examples we simulate the curing process as well as mechanical loading of the cured part with the finite- element-method.*

1 INTRODUCTION

In these days, applications for polymeric materials are found in carbon- and glass fibre-reinforced composite materials, epoxy laminates and (nano-) particle-reinforced polymer structures, cf. RUIZ and TROCHU [1] as well as LANGE [2]. An important production process of fibre-reinforced polymeric (FRP) materials is resin transfer molding (RTM). It is mainly characterized by curing, where the matrix in the initial uncured state, a mixture of resin and curing agent, exhibits a viscous liquid behavior until gelation. The process is highly temperature dependent and influences strongly the mechanical, thermal and chemical properties.

Due to increasing demand, over the last years considerable effort was made to develop three-dimensional constitutive models that account for a time- or degree of cure dependence, respectively, of the mechanical properties. Several suggestions for simulation of polymer curing on the basis of a physically and chemically sound approach have been presented by ADOLF and co-workers, see e.g. [3]. Furthermore, both geometrically linear [4, 5, 6] and nonlinear [7, 3, 8] constitutive models have been proposed by ADOLF *et al.* and HOSSAIN *et al.*, where the latter suggest a thermodynamically consistent framework for the simulation of curing polymers independent of the choice of the free energy density. In this way any phenomenological or micromechanical approach can be utilized. The influence of the fibre/matrix RVE size for a similar model is investigated in HEINRICH *et al.* [9].

In LION and HÖFER [8] a phenomenological thermo-visco-elastic curing model for finite strain deformations is proposed. The formulation is based on process dependent viscosities as in the previous works of HAUPT and LION [10, 11] within a thermodynamic framework. It accounts for thermally and chemically induced volume changes using a ternary multiplicative split of the deformation gradient into mechanical, thermal and chemical parts. Furthermore, a *coordinate of reaction* is introduced representing the degree of cure, and which is taken as in internal variable into the Helmholtz free energy. A advanced application of the finite element method for curing processes is presented in KLINGE *et al.* [12], in order to consider the aspect of microheterogeneity of the curing process by use of a multiscale finite element method.

MAHNKEN and DAMMANN [13] present a three-scale framework for fibre-reinforced polymer curing. It employs a meso-RVE consisting of the fibre and the matrix part and a micro-RVE for the latter consisting of the three components resin, curing agent and solidified material. Microscopic modeling and a comparative study render different *meso bulk material properties* including bounds (for the assumption of a homogeneous mixture for the matrix components) and effective material constants (for the assumption of a heterogeneous arrangement for the matrix components). Based on the preliminaries in [13], in MAHNKEN and DAMMANN [14] a periodic mesostructure is adapted. It is defined by a visco-elastic polymeric matrix and linear-thermo-elastic carbon fibres as a representative unit cell (meso-RVE) subjected to thermo-mechanical loading on the mesoscale. Basic relations in a thermodynamic framework which is specialized to the scenario of a mechanical-thermal-chemical process for polymeric materials are presented. To this end, the effective mesoscopic properties from [13] are applied to the prototype model in [15] resulting in the thermodynamically consistent model in [14].

In this work, we briefly summarize the three-scale framework for FRP curing as well as the *meso bulk properties* for the matrix according to the homogeneous and heterogeneous matrix approaches from [13]. We also outline the meso-model as a result from [14] in combination with the meso to macro transition by volume averaging. Moreover, we investigate the thermo-chemical curing process and subsequent mechanical loading in order to get the *effective bulk properties* for the fully cured composite on the macroscale.

The main aspects and the organization of this paper are summarized as follows: Section 2 introduces the preliminaries for two reaction mechanisms for thermosetting polymers and presents a three-scale framework for fibre reinforced polymer curing. Furthermore, we introduce the meso-RVE consisting of a matrix and a fibre part. Three components of the polymeric matrix are defined and

thus, mass phase fractions are introduced. Based on these preliminaries, two conceptions are distinguished in Section 3. Firstly, an equally distributed mixture on the microscale is assumed, secondly, an arrangement of a heterogeneous microstructure is taken into account. In Section 4 basic relations for the mesoscale are introduced. The constitutive relations of the prototype model including the homogeneous as well as the heterogeneous ansatz for the matrix properties are summarized followed by a comment on the fibre model as a special case. Preliminaries for the computational homogenization scheme which is used for the meso to macro transition are introduced in Section 5. Section 6 presents two numerical examples. In the first example, we illustrate the mechanical-thermo-chemical coupling for a meso-RVE in a three-dimensional finite-element simulation in Subsection 6.1. Some features on the coupling of temperature, curing and visco-elasticity of the proposed model are illustrated for a mesoscopic problem and its homogenized macroscopic response occurring in a curing process. We compare the meso-micro relations for the homogeneous matrix which yield (upper) Voigt and (lower) Reuss bounds with those derived for the heterogeneous matrix which yield effective parameters. Based on the curing process in Subsection 6.1, in the second example in Subsection 6.2 we determine the effective macroscopic anisotropic stiffness tensor and the effective macroscopic anisotropic thermal expansion coefficient for the fully cured fibre reinforced polymer.

Notations

Square brackets $[\bullet]$ are used throughout the paper to denote 'function of' in order to distinguish from mathematical groupings with parenthesis $(\bullet)$.

2 PRELIMINARIES FOR THE CURING OF THERMOSETTING POLYMERS

2.1 Polymerization mechanisms

Epoxy resin systems are included in the group of thermosetting polymers (thermosets). Starting with the initial uncured state the matrix (a mixture of resin and curing agent) undergoes a polymerization process during curing. As introduced by FLORY [16] two polymerization reaction mechanisms are distinguished: 1. by free-radicals or ions (*chain-growth polymerization*) and 2. by functional groups (*step-growth polymerization*).

Considering the scheme of *chain-growth polymerization* shown in Figure 1.a starting with an initiator the unsaturated monomer molecules add onto the active site of a growing polymer chain one

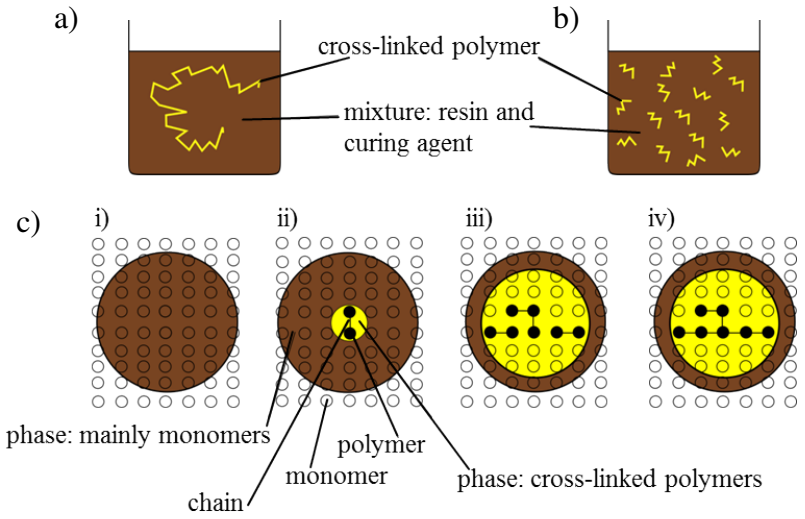

Figure 1: Polymerization in thermosets: a) schematic illustration of chain- and b) step-growth polymerization b) generic representation of a step-growth polymerization adapted to [17] i) uncured state, ii) two monomers react (monomer as predominant species), iii) state with larger chain length including dimer and trimer, iv) state where branching started.

at a time. Different steps operate at different stages of the mechanism (i.e. initiation, propagation, termination, and chain transfer). Following COWIE and ARRIGHI [17], the characteristics of *step-growth polymerization* are the growth throughout the matrix, whereas no initiator is necessary and the reaction between any two functional groups of monomers is stepwise. Thus, at multiple locations and at the same time similar steps are repeated throughout the reaction process as illustrated in Figure 1.b. In particular initiation, propagation and termination reactions are essentially identical in rate and mechanism as shown Figure 1.c. As described in STILLE [18], the chain length increases steadily and random growth takes place as the monomer reacts with both monomer or polymer species with equal ease until a high molecular weight polymer is obtained.

Taking into account both reactions mechanism is the decisive point for two conceptions for the matrix (the *homogeneous matrix* and the *heterogeneous matrix*) we distinguish later on. Especially for the *step-growth polymerization* we assume an idealization: For the locations from where on random growth starts we assume a probabilistic distribution. The random growth is then represented by multiple growing spherical inclusions with its origins at those multiple locations from where on the molecular functional groups of monomers start to react, i.e. the phase of cross-linked monomers in Figure 1.c at one of the multiple locations in Figure 1.b. This region is surrounded by a phase including mainly monomers.

2.2 A three-scale framework for fibre reinforced polymer curing

Based on the polymerization mechanisms described in the previous subsection Figure 2.a gives an overview of the three-scale framework. $\bar{\Pi} \subset \mathcal{R}^3$ denotes the homogeneous macrostructure. It is associated to the periodic mesosstructure $\Pi \subset \mathcal{R}^3$ of a layered fibre reinforced polymer consisting of the matrix part and the fibre part $\Pi = \Pi^M \cup \Pi^F$, respectively, each regarded as homogeneous solid constituents. The mesoscopic representative volume element (meso-RVE) Ω is associated to Π with the decomposition $\Omega = \Omega^M \cup \Omega^F$. We denote by $\boldsymbol{x}^J \subset \Pi^J$ the position vector of a material point $P^J \in \Pi^J$ for which either $J = M$ or $J = F$ holds at time t in the space-time-domain $\Pi^J \times]-\infty, T[$. Here T is the total time of interest. The microstructure $\pi \subset \mathcal{R}^3$ is related to the matrix part Π^M

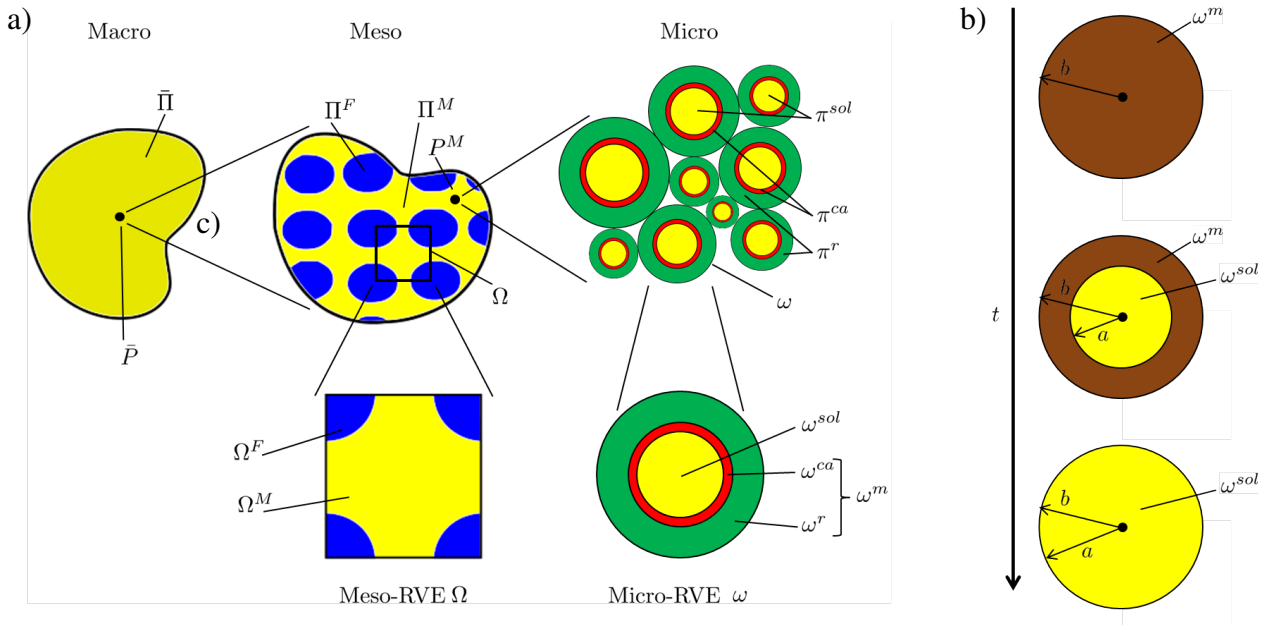

Figure 2: a) Three-scale model showing a homogeneous macroscopic configuration $\bar{\Pi}$, a periodic mesoscopic configuration Π consisting of homogeneous parts Π^F and Π^M, a corresponding meso-RVE Ω and a microscopic configuration as a multiphase system with phases π^{ca}, π^r and π^{sol} and a corresponding micro-RVE ω. b) Micro-RVE as a a two phase composite sphere over time: top) initial uncured, middle) partially cured and bottom) fully cured state.

at every point P^M at time t. $\pi = \pi^{ca} \cup \pi^r \cup \pi^{sol}$ consists of the phases π^j, $j = ca, r, sol$ (curing agent, resin and solidified material), respectively. The representative volume element (micro-RVE) ω is associated to the structure π with a decomposition of the micro-RVE in terms of three components $\omega = \omega^{ca} \cup \omega^r \cup \omega^{sol}$, or for simplification in terms of monomer and fully cured material $\omega = \omega^m \cup \omega^{sol}$. An illustration of such a two-phase system during curing over the time t is given in Figure 2.b.

In the sequel, for notational benefits, we omit the index J, as meso-micro relations are derived only for the behavior of Π^M. Thus, a quantity $\bullet^M$ related to the matrix reads $\bullet$.

2.3 Mass fractions

The matrix Π consists of three phases π^{ca}, π^r and π^{sol}. Following [19], with the time-dependent variables $dm^r[t]$, $dm^{ca}[t]$ and $dm^{sol}[t]$ for the masses of resin, curing agent and solidified material, respectively, the conservation of mass during the curing reaction requires that the masses of all constituents sum up to the total mass of the mixture dm_0. Using this relation, the mass phase fractions of resin, curing agent and solid, $\zeta^r,\ \zeta^{ca},\ \zeta^{sol}$ in Table 1, are introduced such that the sum of all fractions is one.

3 MESOSCOPIC PROPERTIES

Following [13], in order to obtain mesoscopic material properties two different conceptions are presented:

- Homogeneous matrix: An equally distributed mixture on the microscale π is assumed (meso-model hom) for the three constituents which yields bounds for the meso bulk properties.
- Heterogeneous matrix: An arrangement of a heterogeneous microstructure π as shown in Figure 2.a (meso-model het) is taken into account. The microstructure is represented by the two-phase composite sphere as micro-RVE in Figure 2.b with radii a and b which are related to its constituents ω^m and ω^{sol}, respectively.

As a simplification, we assume linear thermo-chemo-elasticity for the microscale π and consequently introduce the heat- and curing-dilatation coefficients α^j and β^j as well as the shear- and compression moduli G^j and K^j for the phases ζ^j, $j = m, sol$. The material parameters are summed up in Table 1, where in addition the degree of cure z is simultaneously defined for the

- Homogeneous matrix: In dependence on the mass phase fractions for the monomer and the solid $\zeta^m[t] = \zeta^r[t] + \zeta^{ca}[t]$, $\zeta^{sol}[t]$.
- Heterogeneous matrix: In dependence on the radii a, b in accordance to the volumes ω^m and ω^{sol} in Figure 2.b.

The justification for this differing formulations is that in [13] for each constituent $m,\ sol$ the authors introduce volume phase fractions as well as mass phase fractions (cf. Table 1) and shown that they almost equal.

The equally distributed mixture yields upper (Voigt) and lower (Reuss) bounds, consequently in total three meso-models $homV,\ homR$ and het which lead to different evolution of the material properties in dependence on the degree of cure z for the mesoscale Π are distinguished in Table 1. The resulting meso-micro relations are summarized for the

- Homogeneous matrix: This meso-model denoted as hom is divided into two sub-models, the
  - Reuss model denoted as $homR$ which yields lower bounds for the meso bulk properties. In particular, we state the *bulk compression modulus* K_R in Table 1, Eq. (5) and the *bulk heat-dilatation coefficient* α_R in Table 1, Eq. (6) in dependence on the degree of cure as well as

the shrinking-dilatation coefficient $\beta(est)$ in Table 1, Eq. (2) which is not dependent on curing. The properties are in agreement with ad hoc assumptions from the literature, i.e. the *bulk curing-dilatation coefficient* corresponds to the derivations by [1], [15] and [20], whereas the *bulk compression modulus* and the *bulk heat-dilatation coefficient* coincide with the well known lower Reuss bounds. Thus, we combine these formulations for the volumetric quantities to a model which we denote as the Reuss model.

– Voigt model denoted as $homV$ which yields upper bounds for the meso bulk properties, in particular the bulk compression modulus K_V in Table 1, Eq. (3) and the bulk heat-dilatation coefficient α_V in Table 1, Eq. (4). This sub-model shares the *bulk curing-dilatation coefficient* in Table 1, Eq. (2) with the Reuss model, as it is constant during curing.

Note, that the sub-models are distinct in view of volumetric quantities, but both share the assumptions for the shear modulus in Table 1, Eq. (1). $G(Adolf)$ coincides basically with the relation given in [21] and applied in [22], [15]. The motivation for the ansatz is that below the gel point z_{gel}, the liquid resin of the matrix is allowing no more than hydrostatic pressure.

- Heterogeneous matrix: This meso-model denoted as het is used to obtain effective meso bulk properties from an analytical solution contrary to bounds for the mixture. In this way, the *composite spheres model* CHRISTENSEN [23], originally providing only an exact solution for the *effective bulk compression modulus* of a heterogeneous medium, is extended to thermal and chemical effects. Thus, the approach in [13] provides the *effective bulk heat-* and *effective curing-dilatation coefficients* α and β which are given in Table 1, Eq. (9) and Eq. (10) in addition to the *effective bulk compression modulus* K in Table 1, Eq. (8). For determination of both, α and β, the quantities L_{th} and L_{cur} are required. They are given in Appendix A, Eq. (A.1) and Eq. (A.2), respectively. We remark, that α and K resulting from the derivations in [13] are in agreement with that in [24] and [23], respectively. Moreover, we assume that the shear modulus is identical to the derivation in [23], [25], [26], [27] as it is not a volumetric quantity which might be affected by the purely volumetric modifications proposed in [13] (even the bulk compression modulus K as volumetric quantity is independent of the modifications in terms of heat- or curing-dilatation). For determination of the shear modulus $G_2(Christ)$ in Table 1, Eq. (8) the coefficients $\mathfrak{A}$, $\mathfrak{B}$, $\mathfrak{C}$ are given in Appendix B, Eq. (A.3) to (A.6).

Remark 1

Due to the upper case in Table 1, Eq. (1), the heterogeneous and homogeneous matrix models already differ in view of the shear modulus for the uncured state $z[0] = 0$:

$$\begin{aligned} &1.\ hom\text{:} \quad G[0 \leq z < z_{\text{gel}}] = 0 \qquad &&\Longrightarrow \quad G[z=0] = 0, \\ &2.\ het\text{:} \quad G^m \leq G[0 \leq z \leq 1] \leq G^{sol} \qquad &&\Longrightarrow \quad G[z=0] = G^m. \end{aligned} \tag{1}$$

4 MESOSCOPIC MODELING

Based on the preliminaries of Section 3 the following exposition is directed to mesoscopic modeling, where we outline the approach in [14], where a general thermodynamic framework is specialized to the scenario of a mechanical-thermal-chemical process for polymeric materials.

4.1 Basic relations for the meso-RVE

The displacement gradient $\nabla \mathbf{u}$ is introduced at each material point P on the mesoscale Π in Figure 2.a. This defines the strain tensor of the geometric linear theory $\boldsymbol{\varepsilon}$ which is additively decomposed

• Mass phase fractions $\quad 1.\ \zeta^m[t] = \zeta^r[t] + \zeta^{ca}[t] = \dfrac{dm^r[t]}{dm_0} + \dfrac{dm^{ca}[t]}{dm_0}, \quad 2.\ \zeta^{sol}[t] = \dfrac{dm^{sol}[t]}{dm_0}$

• Degree of cure $\quad 1.\ \zeta^m = 1 - \dfrac{a^3}{b^3} \qquad 2.\ \zeta^{sol} = 1 - \zeta^m = \dfrac{a^3}{b^3} = z \qquad 3.\ \sum_{j=1}^{2} \zeta^j = 1,$
$4.\ \zeta^j \geq 0, \quad j = m, sol \quad 5.\ \underline{\zeta}_0 = [\zeta^m[0] = 1, \zeta^{sol}[0] = 0]^T$

• Homogeneous matrix (hom)

1. Shear modulus $G(Adolf) = \begin{cases} 0 & z < z_{\text{gel}}, \\ G^{sol}\left(\dfrac{z^2 - z_{\text{gel}}^2}{1 - z_{\text{gel}}^2}\right)^{8/3}, & z \geq z_{\text{gel}} \end{cases}$
2. Curing-dilatation coefficient $\beta(est) = -\beta^m + \beta^{sol}$

Voigt model $(homV)$

3. Compression modulus $K_V = K^m(1-z) + K^{sol}z$
4. Heat-dilatation coefficient $\alpha_V = \dfrac{(1-z)E^m\alpha^m + zE^{sol}\alpha^{sol}}{(1-z)E^m + zE^{sol}}$

Reuss model $(homR)$

5. Compression modulus $K_R = \dfrac{1}{\dfrac{1}{K^m}(1-z) + \dfrac{1}{K^{sol}}z}$
6. Heat-dilatation coefficient $\alpha_R = \alpha^m(1-z) + \alpha^{sol}z$

• Heterogeneous matrix (het)

7. Shear modulus $G_2(Christ) = -\dfrac{G^m\left(\mathfrak{B} - \sqrt{\mathfrak{B}^2 - 4\mathfrak{A}\,\mathfrak{C}}\right)}{2\mathfrak{A}}$
8. Compression modulus $K = K^m + \dfrac{z(K^{sol} - K^m)}{1 + \dfrac{(1-z)(K^{sol} - K^m)}{K^m + \dfrac{4G^m}{3}}}$
9. Heat-dilatation coefficient $\alpha = \dfrac{L_{th}\hat{p} + \dfrac{3K^m}{4G^m}L_{th}\hat{p} - 3K^m\alpha^m}{4G^m}$
10. Curing-dilatation coefficient $\beta = \dfrac{L_{cur}\hat{p} + \dfrac{3K^m}{4G^m}L_{cur}\hat{p} - 3K^m\beta^m}{z4G^m}$

• Material parameters $\underline{\kappa}_{hard} = [K^{sol}, K^m, G^{sol}, G^m, z_{\text{gel}}, \beta^m, \beta^{sol}, \alpha^m, \alpha^{sol}]$

Table 1: Summary and comparison of mesoscopic effective properties and bounds from [13]

into elastic, thermal and chemical parts, $\boldsymbol{\varepsilon}_{el},\ \boldsymbol{\varepsilon}_{th},\ \boldsymbol{\varepsilon}_{cur}$, in Table 2, Eq. (3.1). The volumetric $\boldsymbol{\varepsilon}^{vol}$ and deviatoric parts $\boldsymbol{\varepsilon}^{dev}$ of the strain tensor $\boldsymbol{\varepsilon}$ are defined in in Table 2, Eq. (1). For later use, we apply the *elastic strain tensor* $\boldsymbol{\varepsilon}_{el}$ in Table 2, Eq. (3.1) and define the *elastic volumetric strain* e_{el} in Table 2, Eq.

1. Volumetric and deviatoric strains	$\boldsymbol{\varepsilon}^{vol} = \frac{1}{3}\mathrm{tr}[\boldsymbol{\varepsilon}]\mathbf{1}, \quad \boldsymbol{\varepsilon}^{dev} = \boldsymbol{\varepsilon} - \boldsymbol{\varepsilon}^{vol}$
2. Thermal and shrinking strains	$\boldsymbol{\varepsilon}_{th} = \int_{s=-\infty}^{t} \alpha[s] \frac{d\theta}{ds} ds\mathbf{1},\ \alpha[s] = \left\{ \begin{array}{l} het \\ homV, homR \end{array} \right.$
	$\boldsymbol{\varepsilon}_{cur} = \int_{s=-\infty}^{t} \beta[s] \frac{dz}{ds} ds\mathbf{1},\ \beta[s] = \left\{ \begin{array}{l} het \\ hom \end{array} \right.$
3. (Relative) elastic strain	1. $\boldsymbol{\varepsilon}_{el}[s] = \boldsymbol{\varepsilon}[s] - \boldsymbol{\varepsilon}_{th}[s] - \boldsymbol{\varepsilon}_{cur}[s]$, 2. $e_{el}[s] = \mathrm{tr}\boldsymbol{\varepsilon}_{el}[s]$,
	3. $\boldsymbol{\varepsilon}_t[s] = \boldsymbol{\varepsilon}[s] - \boldsymbol{\varepsilon}[t]$, 4. $e_t[s] = e_{el}[s] - e_{el}[t]$
4. Volumetric stress	$\boldsymbol{\sigma}_{vol} = \int_{s=-\infty}^{t} K[s,t] \frac{d}{ds} e_{el}[s]\ \mathbf{1}\ ds,\ K_0[s,t] = \left\{ \begin{array}{l} het \\ homV, homR \end{array} \right.$
5. Deviatoric stress	$\boldsymbol{\sigma}_{dev} = \int_{s=-\infty}^{t} 2G[s,t] \frac{d}{ds} \boldsymbol{\varepsilon}^{dev}[s] ds$
6. Shear modulus	$G[s,t] = G_0[s] + G_{visco}[s,t],\ G_0[s,t] = \left\{ \begin{array}{l} het \\ hom \end{array} \right.$
7. Curing rate	$\dot{z} = k_A \exp\left(\frac{-E_A}{R\theta}\right) z^a (1-z)^n$
8. Material parameters	$\underline{\kappa}_{kint} = [k_A, E_A, R, a, n, H_T]$
	$\underline{\kappa}_{hard} = [G^m, G^{sol}, \beta^m, \beta^{sol}, K^m, K^{sol}, \alpha^m, \alpha^{sol}]$

Table 2: Constitutive relations for thermo-visco-elasticity and curing for the matrix from [14]

(3.2), which both account for thermal-mechanical and chemical-mechanical coupling. Furthermore, we define the *relative strain tensor* $\boldsymbol{\varepsilon}_t[s]$ and the *relative elastic volumetric strain* e_t in Table 2, Eq. (3.3,4).

4.2 A prototype model for the matrix

The effective mesoscopic properties and bounds summarized in Section 3 (meso-models hom and het) are now applied to the prototype model in [15] to model the matrix as visco-elastic with a coupling to curing. The resulting constitutive relations for the thermal-mechanical-chemical coupled process accounting also for curing are summarized in Table 2, Eq. (1) to Eq. (8), where as in Section 3 two different meso-models are distinguished:

- Homogeneous matrix: According to this assumption the Voigt (upper) and Reuss (lower) bounds for meso bulk material properties are applied. Thus, the sub-models which are summarized in Table 1 $homV$ (Eq. (1)-(4)) and $homR$ (Eq. (1)-(2) and Eq. (5)-Eq. (6)) are employed.
- Heterogeneous matrix: According to this assumption the *effective* meso bulk properties denoted as model het in Table 1 (Eq. (7) -(10)) are employed.

4.2.1 Cure evolution

Following [19], the evolution of the degree of cure is expressed as a function of degree of cure itself in Table 2, Eq. (7), and drives the mass phase fractions $\zeta^m[s]$, $\zeta^{sol}[s]$ in Table 1. It exhibits the property $\dot{z} \geq 0$, where k_A, E_A, R are respectively the Arrhenius constant, the activation energy and the universal gas constant. Furthermore, a, n are power constants.

4.2.2 Stresses

The stress tensor $\boldsymbol{\sigma}$ is obtained by use of a special choice of the Helmholtz free energy which includes the chemically stored energy with respect to curing in [14]. Here, the decomposition $\boldsymbol{\sigma} = \boldsymbol{\sigma}_{vol} + \boldsymbol{\sigma}_{dev}$, is applied, where $\boldsymbol{\sigma}_{vol}$ is the volumetric stress tensor and $\boldsymbol{\sigma}_{dev}$ is the deviatoric stress tensor which are stated in Table 2, Eq. (4) and (5), respectively, and which are be focused in the following two paragraphs.

Firstly, we consider the volumetric part of the stress tensor. Resulting from the decomposition in Table 2, Eq. (3) the stress tensor $\boldsymbol{\sigma}_{vol}$ in Table 2, Eq. (4) is written in terms of the time derivative of the *elastic volumetric strain* e_{el}

$$\frac{d}{ds}e_{el}[s] = \frac{d}{ds}\text{tr}\boldsymbol{\varepsilon}[s] - \frac{d}{ds}\text{tr}\boldsymbol{\varepsilon}_{th}[s] - \frac{d}{ds}\text{tr}\boldsymbol{\varepsilon}_{cur}[s] = \frac{d}{ds}\text{tr}\boldsymbol{\varepsilon}[s] - \frac{d}{ds}(3\alpha[s]\Delta\theta[s]) - \frac{d}{ds}(3\beta[s]z[s]), \quad (5)$$

where $\Delta\theta[s]$ is the temperature change. Although $e_{el}[s]$ takes the same form for both meso-models, however, a difference for the thermal and the curing strains $\boldsymbol{\varepsilon}_{th}$ and $\boldsymbol{\varepsilon}_{cur}$ occurs due to the choice of the meso bulk properties α and β:

- Homogeneous matrix: According to Table 2, Eq. (2), the *weighted* meso bulk curing-dilatation coefficient β for meso-model hom is given in Table 1, Eq. (2). Furthermore, the *weighted* meso bulk heat-dilatation coefficient α for meso-models $homV$ or $homR$ is stated in Table 1, Eq. (4) or Eq. (6), respectively. Due to the use of the quantities from above in the second and third term of the last part in Eq. (5) their time derivatives are required for $\boldsymbol{\sigma}_{vol}$. For details on them see [14].

- Heterogeneous matrix: According to Table 2, Eq. (2), α and β in the third part of Eq. (5) are the *effective* meso bulk properties used in meso-model het of Table 1, Eq. (9) and Eq. (10), respectively, which are also used to define the thermal and the curing strains $\boldsymbol{\varepsilon}_{th}$ and $\boldsymbol{\varepsilon}_{cur}$. The time derivatives of the second and third term for the last part of Eq. (5) are required for the determination of $\boldsymbol{\sigma}_{vol}$ and given in [14].

Moreover, the tensor $\boldsymbol{\sigma}_{vol}$ in Table 2, Eq. (4), is written in terms of the actual compression modulus K which is formulated in terms of the equilibrium compression modulus K_0 and also dependent on one of the underlying assumptions on the microscale. We assume a dependence on the degree of cure for the equilibrium bulk compression modulus K_0:

- Homogeneous matrix: As a consequence of the *weighted* meso bulk properties for $homV$ and $homR$ in Table 1, Eq. (3) or Eq. (5) are applied, respectively.

- Heterogeneous matrix: As a consequence of the *effective* meso bulk property for het in Table 1, Eq. (8) is applied.

Secondly, we consider the deviatoric stress tensor $\boldsymbol{\sigma}_{dev}$ in Table 2, Eq. (5). The shear modulus G for the tensor $\boldsymbol{\sigma}_{dev}$ in Table 2, Eq. (5), is formulated as a Prony series in Table 2, Eq. (6), where G_{visco} accounts for relaxation in dependence on the degree of cure (cf. [28], [22]) and G_0 is the equilibrium shear modulus. We formulate the latter in dependence on one of the underlying assumptions on the microscale and also dependent on the degree of cure:

- Homogeneous matrix: G_0 in Table 2, (6) is defined in Table 1, Eq. (1). For details see [21], [22].

- Heterogeneous matrix: Table 1, Eq. (7), is used for determination of G_0 in Table 2, Eq. (6) as an *effective* meso bulk property. For details see [13].

Finally, required material parameters are collected in the vectors $\underline{\kappa}_{kint}$ and $\underline{\kappa}_{hard}$, in Table 2, Eq. (8).

Remark 2

The degree of cure z occurs in the denominator of the effective bulk curing-dilatation coefficient β in Table 1, Eq. (10). Taking into account the initial state of the degree of cure $z[0] = 0$ dividing by z leads to a singularity of the term. However, if one considers β not on its own account but with regard to the curing strains $\boldsymbol{\varepsilon}_{cur}$ in Table 2, Eq. (2), it becomes clear that the degree of cure z cancels out:

$$\boldsymbol{\varepsilon}_{cur}[z] = \beta z \mathbf{1} = \frac{L_{cur}\hat{p} + \dfrac{3K^m}{4G^m} L_{cur}\hat{p} - 3K^m\beta^m}{z4G^m} z\mathbf{1} = \left(\left(3 + \frac{9K^m}{4G^m} \right) \frac{\hat{p}}{4G^m} L_{cur} - \frac{9K^m\beta^m}{4G^m} \right) \mathbf{1}. \quad (6)$$

4.3 Fibre modeling

For notational benefits, from on this subsection we provide the index $J = M, F$ in order to underline that the quantities stated in the following Section include the behavior of the total fibre-matrix-composite. The fibre $\bullet^F$ in Figure 2.a is considered as a thermo-linear-elastic solid. Consequently it can be modeled as a simplification with the equations for the matrix $\bullet^M$ in Table 2.

5 MESO TO MACRO TRANSITION

The following exposition is directed to the derivation of macroscopic effective properties. For the time being we are interested only in macroscopic *effective properties* for the thermo-linear-elastic fully cured composite. To this end, we denote the instant when the matrix reaches the fully cured state as $t_{z=1} = \min(t[z = 1, \dot{z} = 0)$ and assume from that instant onwards that the macroscopic strain tensor of the geometric linear theory $\bar{\boldsymbol{\varepsilon}}$ is additively decomposed into elastic and thermal parts:

$$\bar{\boldsymbol{\varepsilon}} = \operatorname{sym}\{\nabla \bar{\boldsymbol{u}}\} = \bar{\boldsymbol{\varepsilon}}^{el} + \bar{\boldsymbol{\varepsilon}}^{th}, \quad \text{for } t > t_{z=1}, \quad (7)$$

where $\bar{\boldsymbol{u}}$ is the displacement vector defined at any point $\bar{P}$ of the macrocontinuum $\bar{\Pi}$ in Figure 2.a. Thus, neglecting inelastic effects, we employ the following constitutive equations for the strains in Eq. (7)

$$1.\ \bar{\boldsymbol{\varepsilon}}^{el} = \mathbb{C}^{eff\,-1} \bar{\boldsymbol{\sigma}}, \quad 2.\ \bar{\boldsymbol{\varepsilon}}^{th} = \boldsymbol{A}^{eff} \Delta\bar{\theta}, \quad (8)$$

with the temperature change $\Delta\bar{\theta}$ that takes place uniformly throughout the meso-RVE Ω (which yields $\bar{\theta} = \theta^J$, $J = F, M$). Related matrices in Voigt notation of the *macroscopic effective elasticity tensor* $\mathbb{C}^{eff}$ and the *macroscopic effective heat-dilatation tensor* $\boldsymbol{A}^{eff}$ in Eq. (8) are defined as

$$\begin{aligned} &1.\ \underline{\mathrm{C}}^{eff} = [\underline{\hat{\sigma}}_1, ..., \underline{\hat{\sigma}}_n, ..., \underline{\hat{\sigma}}_6], \ \text{where}\ 2.\ \underline{\hat{\sigma}}_n = [\underline{\hat{\sigma}}_{1n}, ..., \underline{\hat{\sigma}}_{mn}, ..., \underline{\hat{\sigma}}_{6n}]^T, \ \text{for } m, n = 1, ..., 6, \\ &3.\ \underline{\mathrm{A}}^{eff} = [A_1, ..., A_l, ..., A_6]^T, \ \text{for } l = 1, ..., 6. \end{aligned} \quad (9)$$

The tensors $\mathbb{C}^{eff}$, $\boldsymbol{A}^{eff}$ both will be determined by application of a computational homogenization scheme, where the mesostructure variables are related to the homogenized macrocontinuum $\bar{\Pi}$ by use of the *Volume Averaging Theorem*, as formulated in [30]. Based on the decomposition $\Omega = \Omega^M \cup \Omega^F$ in Subsection 2.2 we redefine the overall strains $\bar{\boldsymbol{\varepsilon}}(t)$ and stresses $\bar{\boldsymbol{\sigma}}(t)$ at point $\bar{P}$ in dependence on the mesoscopic strains $\boldsymbol{\varepsilon}$ and stresses $\boldsymbol{\sigma} = \boldsymbol{\sigma}_{vol} + \boldsymbol{\sigma}_{dev}$ (for the meso-RVE $\Omega = \Omega^M \cup \Omega^F$) in Table 2, Eq. (3.1) and Eq. (4-5), respectively:

$$1.\quad \bar{\boldsymbol{\varepsilon}}[t] = \textstyle\sum_J \dfrac{1}{|\Omega^J|} \displaystyle\int_{\Omega^J} \boldsymbol{\varepsilon}^J[t] dV^J, \quad 2.\ \bar{\boldsymbol{\sigma}}[t] = \sum_J \frac{1}{|\Omega^J|} \int_{\Omega^J} \boldsymbol{\sigma}^J[t] dV^J, \ \text{for } J = M,\ F. \quad (10)$$

The main idea is the determination of $\mathbb{C}^{eff}$ and $\boldsymbol{A}^{eff}$ due to prescribed thermal and deformation loadings applied to the unit cell Ω for $t > t_{z=1}$, respectively. In the following, we distinguish between prescribed purely thermal loading for the determination of $\boldsymbol{A}^{eff}$ and prescribed isothermal mechanical loading, i.e. prescribed strains $\hat{\boldsymbol{\varepsilon}}$, for the determination of $\mathbb{C}^{eff}$, where we adapt the approach in [31]. For the determination of $\mathbb{C}^{eff}$ we restrict ourselves to periodic displacement and anti-periodic stress BCs which assure the kinematic compatibility of two neighboring unit cells/meso-RVEs.

6 REPRESENTATIVE EXAMPLES

In this section two numerical examples are presented. In the first example, we illustrate the mechanical-thermo-chemical coupling for a meso-RVE in a three-dimensional finite-element simulation in Subsection 6.1. Here, we apply the material parameters from a parameter identification for a differential scanning calorimetry test (DSC) of an epoxy resin at two temperature rates in [14]. Some features on the coupling of temperature, curing and visco-elasticity of the proposed model in Table 2 are illustrated for a mesoscopic problem and its homogenized macroscopic response occurring in a curing process. On this basis, in the second example in Subsection 6.2 we determine the effective macroscopic anisotropic thermal expansion coefficient and the effective macroscopic anisotropic stiffness tensor for the fully cured fibre reinforced polymer.

6.1 Thermal-mechanical loading during curing of a meso-RVE

In this example, based on the comparative study in [13] for the effective properties and bounds given in Table 1 for $homV$, $homV$, het, some features on the coupling of temperature, curing and visco-elasticity of the proposed model in Table 2 are illustrated for a mesoscopic problem and its homogenized macroscopic response occurring in a curing process. As a simplification for the geometry of a real CFRP (carbon fibre reinforced composite) is shown in Figure 3.a. Here, stiff carbon fibres (blue) embedded in a soft epoxy resin matrix (yellow) are used to model a three dimensional RVE on the mesoscale with a fibre-volume-fraction of 19.6 %. The constitutive response of the stiff fibres is assumed as linear thermo-elastic, cf. Subsection 4.3, while the matrix material is assumed as visco-elastic, hence the meso-models in Table 2 accounting for a homogeneous (hom) and a heterogeneous matrix (het) are applied. Material parameters for the fibres $\underline{\kappa}_{carb}$ in Table 3 are taken from [9], while the remaining ones for the matrix are taken from Table 4. The thermal loading program which is handled as a homogeneously distributed temperature field on the mesoscale is divided into four phases, see θ in Figure 3.b. They are in accordance with the curing process of fibre reinforced composites.

- Phase 1, called HEAT phase: The temperature is increased with constant rate for $0 \leq t \leq 200$ s from the initial value $\theta = 25\ ^\circ C$ to a final value of $\theta = 180\ ^\circ C$.
- Phase 2, called CURE phase: The temperature $\theta = 180\ ^\circ C$ is kept fixed for $200 \leq t \leq 1800$ s.
- Phase 3, called COOL phase: The temperature is decreased from temperature $\theta = 180\ ^\circ C$ at constant rate to room temperature $\bar{\theta} = 25\ ^\circ C$ for $1800 \leq t \leq 2000$ s.
- Phase 4, called HOLD phase: The temperature $\theta = 25\ ^\circ C$ is kept fixed until 10^{15} s.

The displacement boundary conditions of the RVE are statically determined such that free expansion or contraction, respectively, due to thermal loading is possible.

$\underline{\kappa}_{carb}$:	K [MPa]	G [MPa]	α [1/K]
	209091.0	107812.0	$5.6{\cdot}10^{-6}$

Table 3: Values for carbon fibre material parameters (exerpt)

$\underline{\kappa}_{hard}$:	K^m [MPa]	K^{sol} [-]	G^m [MPa]	G^{sol} [-]	β^m [-]	β^{sol} [-]	α^m [1/K]	α^{sol} [1/K]
	150.0	3000.0	120.0	1200.0	0.0	-0.04	$1.5 \cdot 10^{-1}$	$7.5{\cdot}10^{-5}$

Table 4: Values for matrix material parameters (exerpt) in Tables 1 and 2

The thermal-mechanical-chemical coupled problem is solved with the finite element code ”Abaqus/ Standard” [32] by aid of a ”UMAT” subroutine for the meso-models in Table 2. The whole domain

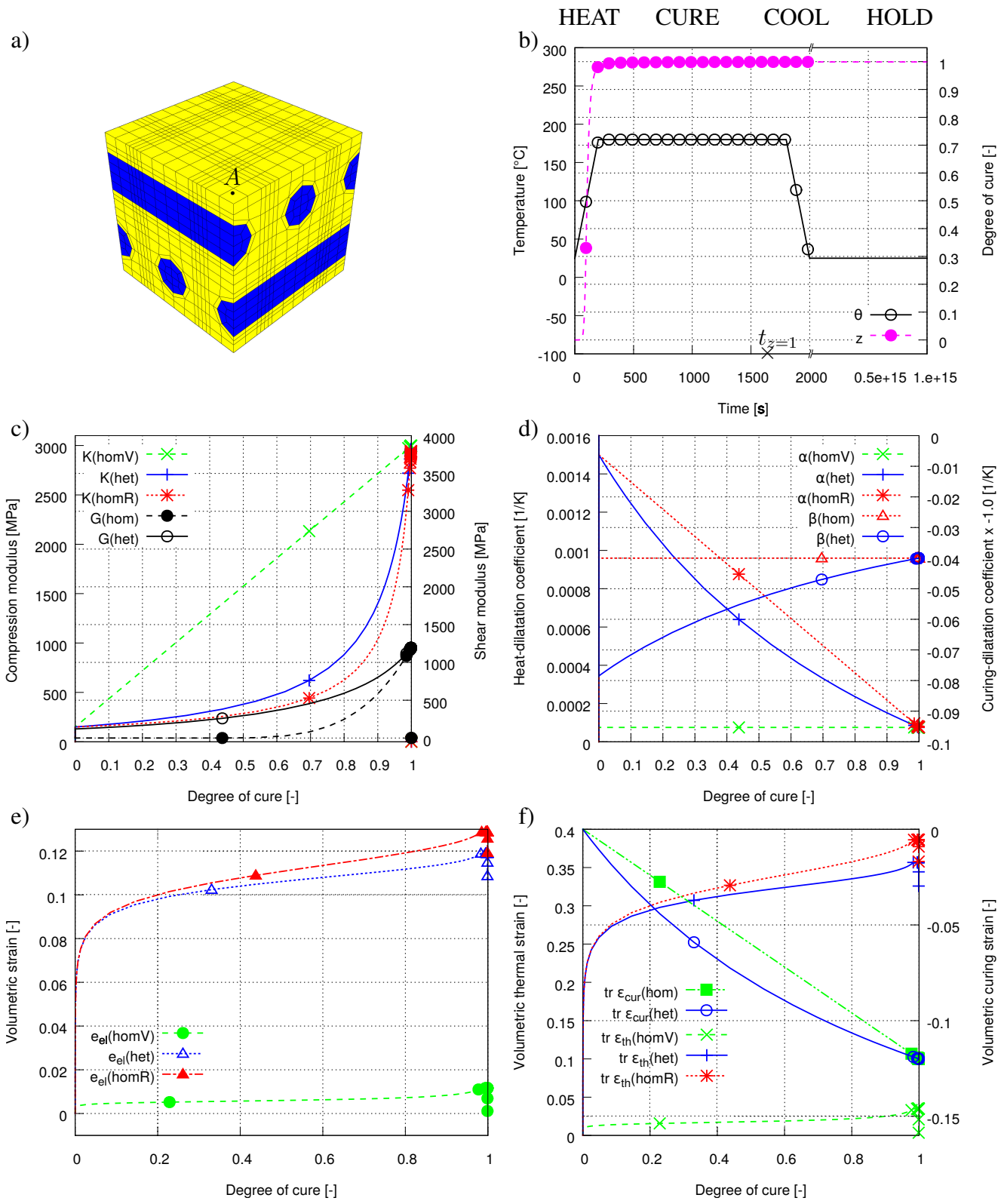

Figure 3: Thermal-mechanical loading during curing of a meso-RVE: a) Geometry with FE-mesh: carbon-fibers (blue) in resin-matrix (yellow) and location of point A considered in the following: b) thermal loading and degree of cure within four phases versus time, c) compression and shear moduli, d) heat- and curing-dilatation coefficients, e) elastic and f) thermal as well as curing volumetric strains versus the degree of cure shown in b).

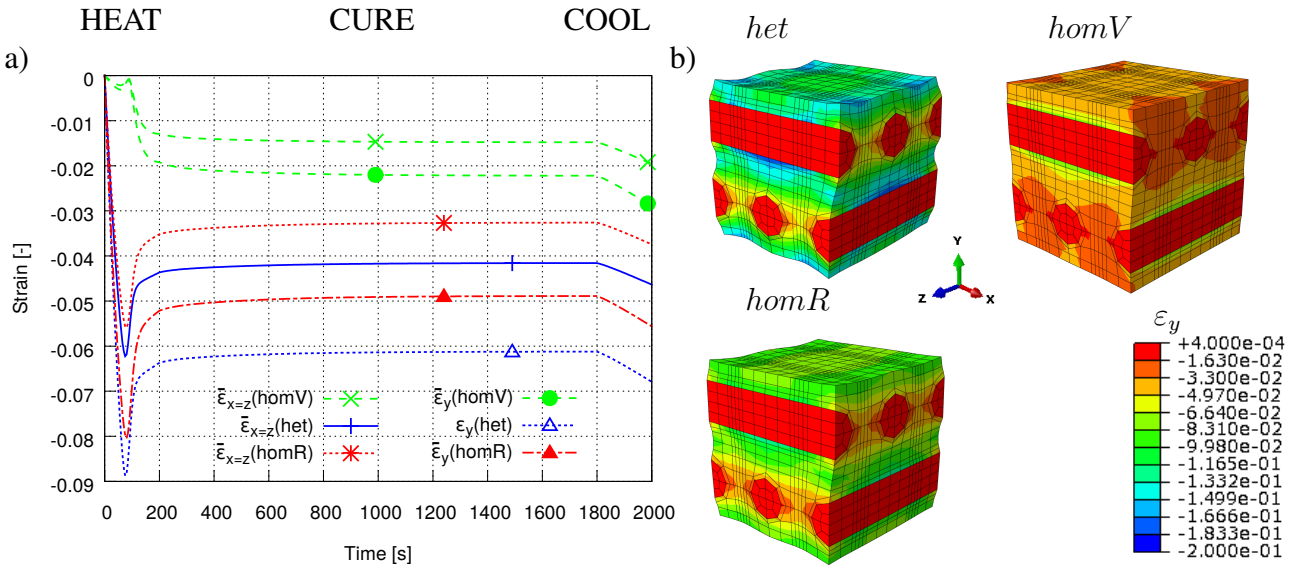

Figure 4: Thermal-mechanical loading during curing of a meso-RVE: a) macroscopic strain vs. time, b) and strain-conturplots resulting from loading program in Figure 3.b for three meso-models for the matrix $homV$, $homR$ and het after phase HOLD

shown in Figure 3.a is discretized using eight node linear hexahedral elements with reduced integration and hourglass control (C3D8R, [32]). Following [33], post processing on the "odb-file" is done using a "PYTHON" script to obtain homogenized quantities on the macro-scale.

Mesoscopic behavior of the matrix at point A

In Figure 3 we summarize some relevant quantities at Point A (in the matrix part) of Figure 3.a resulting from the mechanical-thermal-chemical coupling including the influence of curing and temperature on some material parameters. Figure 3.b shows the degree of cure z at point A versus time. We observe that after the phase CURE the material is fully cured ($z = 1$) which means that the time point $t_{z=1}$ is passed or at least reached. According to the meso-models for $homV$, $homR$ and het the equilibrium shear and bulk moduli Table 2, Eq.(4) and Eq.(6), versus the degree of cure are illustrated in Figure 3.c. Note, that in reality the epoxy behaves like a viscous liquid until gelation at z_{gel} occurs. It is only from that instant onwards that a finite shear modulus is detected. The heat- and curing-dilatation coefficient Table 2, Eq.(2), for the meso-models $homV$, $homR$ and het versus the degree of cure are illustrated in Figure 3.d. As kinematic quantities the volumetric elastic strain tr$\boldsymbol{\varepsilon}_{el}$, the volumetric thermal strain tr$\boldsymbol{\varepsilon}_{th}$ and the volumetric curing strain tr$\boldsymbol{\varepsilon}_{cur}$ are shown for the meso-models $homV$, $homR$ and het versus the degree of cure in Figure 3.e and Figure 3.f.

We observe that the effective meso bulk properties (compression modulus, heat-dilatation coefficient) resulting from meso-model het lie, on the one hand, within the bounds given by meso-models $homV$ and $homR$ and, on the other, within the physically meaningful bounds given by the values for matrix material parameters in Table 4. However, there are two exceptions, the shear modulus for meso-model hom and the curing-dilatation coefficient for meso-model het. The former lies not within the bounds, given by the microscopic material parameters, due to the nature of its definition in Table 1, Eq. (1) (see also Remark 1), the latter shows satisfying results for the shrinkage in Figure 3.d (see also Remark 2) which is in the same physically meaningful region as the shrinkage resulting from meso-model hom and not in contrast to the experimental results in [20].

We conclude, that in the HEAT and CURE phases curing becomes a dominating nonlinear effect, which in combination with the cure-dependent quantities, i.e. the compression and bulk moduli as

well as the dilatation coefficients, renders the strains as nonlinear. The elastic, thermal and curing strains in Figure 3.f do not retain their initial zero value at the fully cured state $t_{z=1}$. This is due to the change of the material properties in Figure 3.c and Figure 3.d. The final, deformed state of the cured RVE is obtained after the HOLD phase. Figure 4.b shows contour plots of the strain component ε_y for each of the meso-models $homV$, $homR$ and het. We observe that for each meso-model a different eigenstrain state remains. Meso-model $homV$ has the lowest amount of eigenstrain in the matrix, moderate eigenstrains are observed in the matrix where meso-model $homR$ is used and very inhomogeneous eigenstrains occur in the matrix accompanied with meso-model het.

Macroscopic behavior of the meso-RVE

Applying Eq. (10.1), homogenization leads to results on the less resolved macroscale. In Figure 4.a the components $\bar{\varepsilon}_{x,y,z}(homV), \bar{\varepsilon}_{x,y,z}(homR), \bar{\varepsilon}_{x,y,z}(het)$ of the macroscopic strain resulting from each meso-model are shown whereas the shear components remain zero at all and therefore are left out. In particular, shrinking due to the degree of cure is observed in phases HEAT and CURE. The macroscopic strains represent an orthotropic behavior due to the geometry of the meso-RVE. After the COOL phase there are remaining macroscopic (eigen-)strains. The amount is dependent on the chosen meso-model $homV$, $homR$ or het.

6.2 Effective properties of a meso-RVE after curing

For the meso-RVE from Section 6.1 a state with (meso- and macroscopic) eigenstrains after the phase HOLD (cf. Figure 3) at $t = 10^{15} > t_{z=1}$ remains which differs for each of the meso-models $homV$, $homR$ and het. Thus, we define the macroscopic strain state for each meso-model using Eq. (10.1): $\bar{\boldsymbol{\varepsilon}}^{\text{HOLD}}(k) = \bar{\boldsymbol{\varepsilon}}(k, t = 10^{15})$, for $k = homV,\ homR,\ het$. In the following, based on the loading program of Subsection 6.1, the effective properties for the fully cured meso-RVE are determined in a two-part example. In particular we determine the macroscopic thermal expansion tensor following an approach in [34] and the elastic stiffness tensor for $t > t_{z=1}$ following an approach in [31]. Therefore, the meso-RVE is subjected to two cases of second loadings, the purely thermal and the purely mechanical loading.

Macroscopic anisotropic thermal expansion tensor

The the meso-RVE with statically determined displacement boundary conditions is subjected to purely thermal second loading in this first part of the two-part example. For

- Phase 5, called THERM2 phase: The temperature is increased with constant rate in a time period of 10^{-6} s from $\theta = 25\ ^\circ C$ to a final value of $\theta = 26\ ^\circ C$ (temperature unit loading, $\theta = \bar{\theta} \Longrightarrow \Delta\bar{\theta} = 1$, as shown in Figure 5.a).

Insertion of Eq. (8) into Eq. (7) with the conditions of purely thermal loading of phase THERM2 in combination with the statically determined BCs yields:

$$\bar{\boldsymbol{\varepsilon}} - \bar{\boldsymbol{\varepsilon}}^{\text{HOLD}} = \bar{\boldsymbol{\varepsilon}}^{th} = \boldsymbol{A}^{eff} \Delta\bar{\theta}. \tag{11}$$

Next, we define the macroscopic strain state after the loading THERM2 by use of Eq. (10.1) as $\bar{\boldsymbol{\varepsilon}}^{\text{THERM2}}(k)$, for $k = homV,\ homR,\ het$. Exchanging the left term of Eq. (11) by $\bar{\boldsymbol{\varepsilon}}^{\text{THERM2}}(k)$ gives the coefficients for the anisotropic thermal expansion tensor in Eq. (9): $\bar{\boldsymbol{\varepsilon}}^{\text{THERM2}}(k) = \boldsymbol{A}^{eff}(k)$, for $k = homV,\ homR,\ het$. The effective thermal expansion tensor in matrix representation $\underline{\mathrm{A}}^{eff}(k)$ for the meso-models k is shown in Table 5. We conclude that $\boldsymbol{A}^{eff}(k)$ is almost independent of the eigenstrains resulting from models $k = homV,\ homR,\ het$. Additionally, we remark, that the assumption of linear thermo-elasticity on the macroscale (which leads to Eq.(7)) is justified for small temperature changes and time increments, i.e. phase THERM2.

Meso-model	A_1 [1/K]	A_2 [1/K]	A_3 [1/K]	A_4 [1/K]	A_5 [1/K]	A_6 [1/K]
$\underline{\mathrm{A}}^{eff}(homV)$	$1.178 \cdot 10^{-5}$	$1.640 \cdot 10^{-5}$	$1.179 \cdot 10^{-5}$	$4.636 \cdot 10^{-10}$	$7.064 \cdot 10^{-10}$	$1.023 \cdot 10^{-9}$
$\underline{\mathrm{A}}^{eff}(homR)$	$1.174 \cdot 10^{-5}$	$1.649 \cdot 10^{-5}$	$1.191 \cdot 10^{-5}$	$1.209 \cdot 10^{-9}$	$1.936 \cdot 10^{-9}$	$1.916 \cdot 10^{-9}$
$\underline{\mathrm{A}}^{eff}(het)$	$1.173 \cdot 10^{-5}$	$1.646 \cdot 10^{-5}$	$1.181 \cdot 10^{-5}$	$8.559 \cdot 10^{-10}$	$2.424 \cdot 10^{-9}$	$4.567 \cdot 10^{-9}$

Table 5: Effective properties of a meso-RVE after curing: Macroscopic effective thermal expansion matrices $\underline{\mathrm{A}}^{eff}(k)$ of Eq. (9) for $k = homV, homR, het$) resulting from second loading in phase THERM2 as shown in Figure 5.a

Macroscopic anisotropic elastic stiffness tensor

The meso-RVE with periodic displacement boundary conditions is subjected to purely mechanical second loading in this second part of the two-part example. For

- Phase 5, called MECH phase: The macroscopic strain is prescribed at constant rate in a time period of 10^{-6} s with six different prescribed macroscopic strains in Voigt notation $\hat{\underline{\varepsilon}}_x = [10^{-3}, 0, 0, 0, 0, 0]^T$,..., $\hat{\underline{\varepsilon}}_{yz} = [0, 0, 0, 0, 0, 10^{-3}]^T$ (mechanical loading shown in Figure 5.b).

Insertion of Eq. (8) into Eq. (7) with the conditions of purely mechanical loading of phase MECH yields

$$\bar{\boldsymbol{\varepsilon}} - \bar{\boldsymbol{\varepsilon}}^{\mathrm{HOLD}} = \bar{\boldsymbol{\varepsilon}}^{el} = \mathbb{C}^{eff\,-1}\bar{\boldsymbol{\sigma}}. \tag{12}$$

Additionally, from Eq. (10.1) in combination with the prescribed macroscopic strains (cf. Section 5) one gets

$$\bar{\boldsymbol{\varepsilon}} - \bar{\boldsymbol{\varepsilon}}^{\mathrm{HOLD}} = \hat{\boldsymbol{\varepsilon}}_n, \text{ for } n = x, ..., yz. \tag{13}$$

Rearrangement of Eq. (12) and insertion Eq. (13) as well as taking into account the definition for $\underline{\mathrm{C}}^{eff}$ in Eq. (9.1) results into the following matrix representation in Voigt notation

$$\underline{\mathrm{C}}^{eff}\hat{\underline{\varepsilon}}_n = [\hat{\underline{\sigma}}_1, ..., \hat{\underline{\sigma}}_n, ..., \hat{\underline{\sigma}}_6]\hat{\underline{\varepsilon}}_n = \bar{\underline{\sigma}}(\hat{\underline{\varepsilon}}_n), \text{ for } n = x, ..., yz, \tag{14}$$

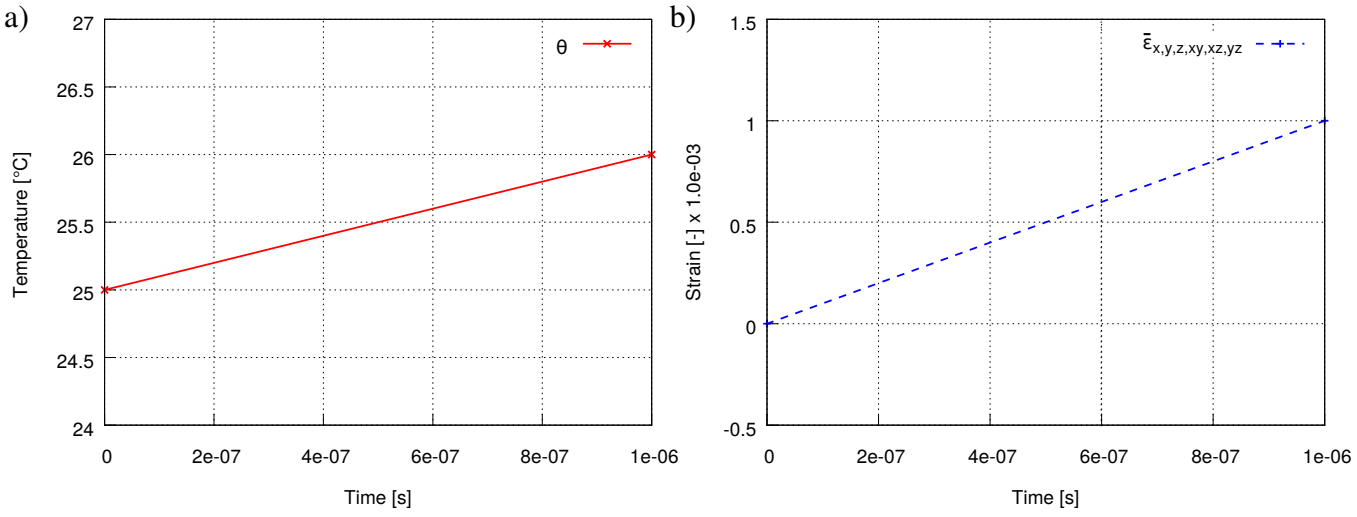

Figure 5: Effective properties of a meso-RVE after curing: Determination due to: a) thermal (THERM2) and b) mechanical (MECH) loading of the meso-RVE

Meso-model	$\underline{\hat{\sigma}}_1$ [MPa]	$\underline{\hat{\sigma}}_2$ [MPa]	$\underline{\hat{\sigma}}_3$ [MPa]	$\underline{\hat{\sigma}}_4$ [MPa]	$\underline{\hat{\sigma}}_5$ [MPa]	$\underline{\hat{\sigma}}_6$ [MPa]
$\underline{\mathbf{C}}^{eff}(homV)$	$6.082 \cdot 10^4$	$1.124 \cdot 10^3$	$9.076 \cdot 10^2$	$4.105e-02$	$6.104 \cdot 10^{-5}$	$-1.221 \cdot 10^{-4}$
	$1.124 \cdot 10^3$	$9.893 \cdot 10^3$	$1.124 \cdot 10^3$	$-1.328 \cdot 10^{-2}$	$1.709 \cdot 10^{-3}$	$1.495 \cdot 10^{-3}$
	$9.076 \cdot 10^2$	$1.124 \cdot 10^3$	$6.082 \cdot 10^4$	$4.883 \cdot 10^{-4}$	$9.155 \cdot 10^{-5}$	$1.831 \cdot 10^{-4}$
	$4.134 \cdot 10^{-2}$	$-1.491 \cdot 10^{-2}$	$2.507 \cdot 10^{-4}$	$4.385 \cdot 10^3$	$-1.026 \cdot 10^{-3}$	$2.915 \cdot 10^{-6}$
	$1.229 \cdot 10^{-4}$	$2.771 \cdot 10^{-6}$	$2.041 \cdot 10^{-5}$	$-9.907 \cdot 10^{-4}$	$4.647 \cdot 10^3$	$2.239 \cdot 10^{-4}$
	$-3.363 \cdot 10^{-5}$	$-5.244 \cdot 10^{-4}$	$-4.238 \cdot 10^{-4}$	$2.185 \cdot 10^{-6}$	$2.756 \cdot 10^{-4}$	$4.385 \cdot 10^3$
$\underline{\mathbf{C}}^{eff}(homR)$	$6.082 \cdot 10^4$	$1.124 \cdot 10^3$	$9.076 \cdot 10^2$	$4.192 \cdot 10^{-2}$	$9.308 \cdot 10^{-4}$	$7.477 \cdot 10^{-4}$
	$1.124 \cdot 10^3$	$9.893 \cdot 10^3$	$1.124 \cdot 10^3$	$-1.494 \cdot 10^{-2}$	$1.526 \cdot 10^{-4}$	$-1.688 \cdot 10^{-4}$
	$9.076 \cdot 10^2$	$1.124 \cdot 10^3$	$6.082 \cdot 10^4$	$3.052 \cdot 10^{-4}$	$4.120 \cdot 10^{-4}$	$0.000 \cdot 10^0$
	$4.134 \cdot 10^{-2}$	$-1.495 \cdot 10^{-2}$	$2.522 \cdot 10^{-4}$	$4.385 \cdot 10^3$	$-9.682 \cdot 10^{-4}$	$2.279 \cdot 10^{-6}$
	$1.231 \cdot 10^{-4}$	$1.397 \cdot 10^{-6}$	$2.007 \cdot 10^{-5}$	$-1.004 \cdot 10^{-3}$	$4.647 \cdot 10^3$	$2.642 \cdot 10^{-4}$
	$-3.489 \cdot 10^{-5}$	$-3.963 \cdot 10^{-4}$	$-4.342 \cdot 10^{-4}$	$2.204 \cdot 10^{-6}$	$3.073 \cdot 10^{-4}$	$4.385 \cdot 10^3$
$\underline{\mathbf{C}}^{eff}(het)$	$6.082 \cdot 10^4$	$1.124 \cdot 10^3$	$9.075 \cdot 10^2$	$4.021 \cdot 10^{-2}$	$-3.204 \cdot 10^{-4}$	$-1.068 \cdot 10^{-4}$
	$1.124 \cdot 10^3$	$9.893 \cdot 10^3$	$1.124 \cdot 10^3$	$-1.314 \cdot 10^{-2}$	$1.434 \cdot 10^{-3}$	$1.114 \cdot 10^{-3}$
	$9.076 \cdot 10^2$	$1.124 \cdot 10^3$	$6.082 \cdot 10^4$	$1.053 \cdot 10^{-3}$	$5.493 \cdot 10^{-4}$	$3.815 \cdot 10^{-4}$
	$4.135 \cdot 10^{-2}$	$-1.491 \cdot 10^{-2}$	$2.513 \cdot 10^{-4}$	$4.385 \cdot 10^3$	$-1.039 \cdot 10^{-3}$	$2.297 \cdot 10^{-6}$
	$1.231 \cdot 10^{-4}$	$1.829 \cdot 10^{-6}$	$2.034 \cdot 10^{-5}$	$-1.021 \cdot 10^{-3}$	$4.647 \cdot 10^3$	$2.418 \cdot 10^{-4}$
	$-3.515 \cdot 10^{-5}$	$-4.418 \cdot 10^{-4}$	$-4.605 \cdot 10^{-4}$	$2.498 \cdot 10^{-6}$	$2.809 \cdot 10^{-4}$	$4.385 \cdot 10^3$

Table 6: Effective properties of a meso-RVE after curing: Macroscopic effective stiffness matrices $\underline{\mathbf{C}}^{eff}$ of Eq. (9) for $k = homV, homR, het$) resulting from second loading in phase MECH as shown in Figure 5.b

where $\bar{\underline{\sigma}}(\hat{\underline{\varepsilon}}_n)$ are the stresses in Eq. (10.2) in Voigt notation resulting from the prescribed macroscopic strains in Voigt notation $\hat{\underline{\varepsilon}}_n$. For example for $n = x$ one gets

$$\underline{\mathbf{C}}^{eff}\hat{\underline{\varepsilon}}_x = \underline{\mathbf{C}}^{eff}[1,0,0,0,0,0]^T \cdot 10^{-3} = \hat{\underline{\sigma}}_1 \cdot 10^{-3} = [\hat{\underline{\sigma}}_{11}, ..., \hat{\underline{\sigma}}_{61}]^T \cdot 10^{-3} = \bar{\underline{\sigma}}(\hat{\underline{\varepsilon}}_x). \tag{15}$$

Taking into account the right-hand side of Eq. (15) we conclude that the n-th column of $\underline{\mathbf{C}}^{eff}$, denoted as $\hat{\underline{\sigma}}_n$, can be obtained due to the six prescribed macroscopic strains $\hat{\boldsymbol{\varepsilon}}_n$ in phase MECH, where $n = 1, ...6$. Consequently, proceeding in the same manner as in Eq. (15) for each of the meso-models $k = homV,\ homR,\ het$ gives the effective stiffness tensor in matrix representation $\underline{\mathbf{C}}^{eff}(k)$ which is shown in Table 6. We conclude that $\mathbb{C}^{eff}$ is almost independent of the eigenstrains resulting from models $k = homV,\ homR,\ het$. Moreover, we remark, that the assumption of linear thermo-elasticity on the macroscale (which leads to Eq. (7)) is justified for small strain and time increments, i.e. phase MECH.

7 CONCLUSIONS

In this paper, we applied a three-scale framework for fibre-reinforced polymer curing from [13]. The three-scale framework employs a meso-RVE consisting of the fibre and the matrix part and a micro-RVE for the latter consisting of the three components resin, curing agent and solidified material. The meso bulk properties in dependence on mass phase fractions resulting from the micro-RVE are taken from [13]. Thus, Voigt and Reuss bounds as well as effective properties are determined for the assumptions of a homogeneous and a heterogeneous matrix, respectively. In [14] those properties are incorporated into a mesoscopic constitutive model for temperature-dependent visco-elastic effects accompanied by curing which is summarized in this work. Thus, the incorporation of the meso

bulk properties, in particular the meso bulk compression and shear moduli as well as the heat- and shrinking-dilatation coefficients for the homogeneous as well as for the heterogeneous matrix, into a visco-elastic model with a coupling to curing [15] is outlined.

The simulation of the curing process for the meso-RVE subjected to mechanical-thermal-chemical loading demonstrates the capability of the model to simulate this process. The effect of anisotropic material behavior due to the incorporation of fibres into the polymeric matrix is constituted on the macroscale. Both, on the mesoscale, as well as on the macroscale the distinction between the homogeneous and the heterogeneous matrix assumption for the determination of the effective mesoscopic material properties influences the remaining eigenstrains.

Concerning further extensions, the meso bulk properties should also consider visco-elastic effective properties and a generalization for the *n-layered composite spheres model* in [27] could be taken into account. Taking the simulation of large-scale engineering finite-element structures into account, the meso to macro transition should be taken into account during the total curing process and parameter identification should be accomplished to obtain material properties or the visco-elastic model.

Acknowledgement

This work is based on investigations of the "SPP 1712 - Intrinsische Hybridverbunde fr Leichtbautragstrukturen", which is kindly supported by the Deutsche Forschungsgemeinschaft (DFG).

Appendix

In accordance with [13] for Table 1, equations (9), (10) and (8), respectively, we use the definitions

$$L_{th} = \frac{4\,G^m\,\left(3\,\alpha^m\;K^{sol}\,K^m+4\,z\,\alpha^{sol}\,K^{sol}\,G^m-4\,z\,\alpha^m\,K^m\,G^m+4\,\alpha^m\;K^m\,G^m\right)}{\hat{p}\;\left(4\,z\,K^{sol}\,G^m-4\,z\,K^m\,G^m+4\;K^m\,G^m+3\;K^{sol}\,K^m\right)}, \tag{A.1}$$

$$L_{cur} = \frac{4\,G^m\,\left(3\,\beta^m\;K^{sol}\,K^m+4\,z\,\beta^{sol}\,K^{sol}\,G^m-4\,z\,\beta^m\,K^m\,G^m+4\,\beta^m\;K^m\,G^m\right)}{\hat{p}\;\left(4\,z\,K^{sol}\,G^m-4\,z\,K^m\,G^m+4\;K^m\,G^m+3\;K^{sol}\,K^m\right)}, \tag{A.2}$$

and

$$\begin{aligned}\mathfrak{A} &= \eta_2\,z^{\frac{5}{3}}\,\left(\frac{252\,G^{sol}}{G^m}-252\right)-\eta_2\,\eta_3\;\left(40\,\nu^m-28\right)-z^{\frac{7}{3}}\,\left(4\,\eta_1\,\eta_3+2\,\eta_2\,\left(\frac{63\,G^{sol}}{G^m}-63\right)\right)\\ &-\eta_2\,z\,\left(\frac{50\,G^{sol}}{G^m}-50\right)\,\left(8\,\nu^{m2}-12\,\nu^m+7\right)-\eta_1\,z^{\frac{10}{3}}\,\left(\frac{8\,G^{sol}}{G^m}-8\right)\,\left(5\,\nu^m-4\right)\end{aligned} \tag{A.3}$$

$$\begin{aligned}\mathfrak{B} &= z^{\frac{7}{3}}\,\left(4\,\eta_1\,\eta_3+2\,\eta_2\,\left(\frac{63\,G^{sol}}{G^m}-63\right)\right)+\eta_2\,\eta_3\,\left(\frac{45\,\nu^m}{2}-\frac{21}{2}\right)-\eta_2\,z^{\frac{5}{3}}\,\left(\frac{252\,G^{sol}}{G^m}-252\right)\\ &+\eta_1\,z^{\frac{10}{3}}\,\left(\frac{2\,G^{sol}}{G^m}-2\right)\,\left(5\,\nu^m-1\right)-\eta_2\,\nu^m\,z\,\left(\frac{75\,G^{sol}}{G^m}-75\right)\,\left(\nu^m-3\right)\end{aligned} \tag{A.4}$$

$$\begin{aligned}\mathfrak{C} &= \eta_2\,z^{\frac{5}{3}}\,\left(\frac{252\,G^{sol}}{G^m}-252\right)-\eta_2\,\eta_3\;\left(5\,\nu^m+7\right)-z^{\frac{7}{3}}\,\left(4\,\eta_1\,\eta_3+2\,\eta_2\,\left(\frac{63\,G^{sol}}{G^m}-63\right)\right)\\ &+\eta_2\,z\,\left(\frac{25\,G^{sol}}{G^m}-25\right)\,\left(\nu^{m2}-7\right)+\eta_1\,z^{\frac{10}{3}}\,\left(\frac{4\,G^{sol}}{G^m}-4\right)\,\left(5\,\nu^m-7\right),\end{aligned} \tag{A.5}$$

where

$$\begin{aligned}1.\;\eta_1 &= 105\,\nu^{sol}-105\,\nu^m-\left(\frac{G^{sol}}{G^m}-1\right)\,\left(5\,\nu^{sol}+7\right)\,\left(10\,\nu^m-7\right),\\ 2.\;\eta_2 &= \left(\frac{G^{sol}}{G^m}-1\right)\,\left(5\,\nu^{sol}+7\right)-35\,\nu^{sol}+35,\\ 3.\;\eta_3 &= 15-\left(\frac{G^{sol}}{G^m}-1\right)\,\left(10\,\nu^m-8\right)-15\,\nu^m.\end{aligned} \tag{A.6}$$

REFERENCES

[1] E. RUIZ, F. TROCHU, Thermomechanical properties during cure of glass-polyester RTM composites: elastic and viscoelastic modeling, *J. Compos. Mater.*, **39**, 881-916, 2005

[2] J. LANGE, Viscoelastic properties and transitions during thermal and UV cure of a methacrylate resin, *Polym. Eng. Sc.*, **39**, 1651-1660, 1999

[3] D.B. ADOLF, R.S. CHAMBERS, J.M. CARUTHERS, Extensive validation of a thermodynamically consistent, nonlinear viscoelastic model for glassy polymers, *Polymer*, **45**, 4599-4621, 2004

[4] D.B. ADOLF, R.S. CHAMBERS, Verification of the capability for quantitative stress prediction during epoxy cure, *Polymer*, **38**, 5481-5490, 1997

[5] D.B. ADOLF, J.E. MARTIN, R.S. CHAMBERS, S.N. BURCHETT, T.R. GUESS, Stresses during thermoset cure, *J. Mater. Res.*, **13**, 530-550, 1998

[6] M. HOSSAIN, G. POSSART, P. STEINMANN, A small-strain model to simulate the curing of thermosets, *Comput. Mech.*, **43**(6), 769-779, 2009

[7] D.B. ADOLF, R.S. CHAMBERS, A thermodynamically consistent, nonlinear viscoelastic approach for modeling thermosets during cure, *J. Rheol.*, **51**, 23-50, 2007

[8] M. HOSSAIN, G. POSSART, P. STEINMANN, A finite strain framework for the simulation of polymer curing, *Comput. Mech.*, **44**, 621-630, 2009

[9] C. HEINRICH, M. ALDRIDGE, A.S. WINEMAN, J. KIEFFER, A. M. WAAS AND K. SHAHWAN, The influence of the representative volume element (RVE) size on the homogenized response of cured fibre composites. *Model. Simul. Materi. Sc.*, **20**, 75007, 2012

[10] P. HAUPT, A. LION, On finite linear viscoelasticity of incompressible isotropic materials, *Acta Mech.*, **159**, 87-124, 2002

[11] A. LION, On the large deformation behaviour of reinforced rubber at different temperatures, *J. Mech. Phys. Solids*, **45**, 1805-1834, 1997

[12] S. KLINGE, A. BARTELS, P. STEINMANN, Modeling of curing processes based on a multi-field potential. Single- and multiscale aspects, *Int. J. Solids Struct.*, **49**, 2320-2333, 2012

[13] R. MAHNKEN, C. DAMMANN, A three-scale framework for fibre-reinforced-polymer curing coupled to visco-elasticity Part I: Microscopic modeling and mesoscopic effective properties, submitted to *Int. J. Solids Struct.*, 2015

[14] R. MAHNKEN, C. DAMMANN, A three-scale framework for fibre-reinforced-polymer curing coupled to visco-elasticity Part II: Mesoscopic modeling and macroscopic effective properties, submitted to *Int. J. Solids Struct.*, 2016

[15] R. MAHNKEN, Thermodynamic consistent modeling of polymer curing coupled to viscoelasticity at large strains, *Int. J. Solids Struct.*, **50**(13), 2003-2021, 2013

[16] P. J. FLORY, Principles of Polymer Chemistry, *Cornell University Press*, 1953

[17] J.M.G. COWIE, V. ARRIGHI, Polymers: Chemistry and Physics of Modern Materials, *CRC Press*, New York, 2007

[18] J. K. STILLE: Step-Growth Polymerization, *Journal of Chemical Education*, **58**(11), 862-866, 2005

[19] A. LION, P. HÖFER, On the phenomenological representation of curing phenomena in continuum mechanics, *Arch. Mech.*, **59**, 59-89, 2007

[20] R. HILL; S. V. MUZUMDAR; L. J. LEE, Analysis of Volumetric Changes of Unsaturated Polyester Resins During Curing, *Polym. Eng. Sci.*, **35**(10), 852-859, 1995

[21] D.B. ADOLF, J.E. MARTIN, Calculation of stresses in crosslinking polymers, *J. Compos. Mater.*, **30**, 13-34, 1996

[22] M.H.H. MEUWISSEN, H.A. DE BOER, H. L.A.H. STEIJVERS, P.J.G. SCHREURS, M.G.D. GEERS, Residual stresses in microelectronics induced by thermoset packaging materials during cure, *Microelectro. Relia.*, **44**, 1985-1994, 2004

[23] R. M. CHRISTENSEN, *Mech.Compos. Mater.*, John Wiley and Sons, New York, 1979

[24] A. GUSEV, Effective coefficient of thermal expansion of n-layered composite sphere model: Exact solution and its finite element validation. *Int. J. Eng. Sci.*, **84**, 54-61, 2014

[25] R. M. CHRISTENSEN, K. H. LO, Solutions for effective shear properties in three phase sphere and cylinder models, *J. Mech. Phys. Solids*, **27**(4), 315-330, 1979

[26] R. M. CHRISTENSEN, A critical evaluation for a class of micromechancis models, *Mech. Phys. Solids*, **38**(3), 379-404, 1990

[27] E. HERVE, A. ZAOUI, N-layered inclusion based micromechanical modeling. *Int. J. Eng. Sc.*, **31**(1), 1-10, 1993

[28] J.E. MARTIN, D.B. ADOLF, Constitutive equation for cure-induced stresses in a viscoelastic material, *Macromolecules*, **23**, 5014-5019, 1990

[29] M.L. WILLIAMS, R.F. LANDEL, J.D. FERRY, The temperature dependence of relaxation mechanisms in amorphous polymers and other glass-forming liquids, *J. American Chem. Soc.*, **14**, 3701-3707, 1955

[30] R. HILL, On constitutive macro-variables for heterogeneous solids at finite strain, *Proc. R. Soc. London, A, Mathematical and Physical Sciences*, **326**(1565), 131-147, 1972

[31] M. KÄSTNER, *Skalenbergreifende Modellierung und Simulation des mechanischen Verhlatens von textilverstärktem Polypropylen unter Nutzung der XFEM*, Dissertation, TU Dresden, 2009

[32] ABAQUS, Dassault Systemes Simulia Corp.: *Theory manual - Version 6.13-1*, Providence, RI, USA, 2013

[33] E.J. BARBERO, Finite Element Analysis of Composite Materials using Abaqus. Composite Materials: Design and Analysis, *Crc. Pr. Inc.*, 2013

[34] C. DAMMANN, R. MAHNKEN, Mesoscopic modelling of the RTM process for homogenization, In: *Coupled Problems in Science and Enfgineering* **VI**, 713-724, Eds. B. Schrefler, E. Onate, M. Papadrakakis, 2015